JOURNAL OF PROPULSION AND POWER
Vol. 19, No. 3, May–June 2003

Characteristics and Control of Combustion Instabilities in a Swirl-Stabilized Spray Combustor

S. Acharya,* S. Murugappan,† M. O'Donnell,† and E. J. Gutmark‡
Louisiana State University, Baton Rouge, Louisiana 70803

Active control of combustion instabilities in a swirl-stabilized spray combustor was investigated. The combustor was characterized by a thermoacoustic instability at approximately 200 Hz. Both open- and closed-loop control tests were conducted. A feedback phase-delay control was implemented using a high-speed microprocessor. The phase-delay control clearly indicates the potential for suppressing the thermoacoustic instabilities in swirl-stabilized combustion. Two flow conditions, one corresponding to high NOx and another corresponding to high-pressure oscillations, were selected for feedback-loop control studies. Best control was achieved with 60–90 deg phase lag, and for the high-pressure oscillation baseline case, the peak amplitude of the pressure oscillations decrease by a factor of three. It was observed that control of pressure oscillations could be achieved without adversely effecting or increasing the NOx emissions. In fact, NOx emissions decrease with control. Velocity measurements were performed for both the uncontrolled and controlled conditions using a two-component laser Doppler velocimeter system. With control, the rms values of the velocity fluctuations decrease significantly (over 50% in certain regions), and this reduction is observed in both the coherent and random components of the velocity fluctuations. Control also leads to an increase in the strength of the central recirculation region, which promotes flame stability.

Nomenclature

D	=	combustor inner diameter
P_{atm}	=	atmospheric pressure
P''	=	instantaneous pressure fluctuations
p'_{rms}	=	rms of pressure fluctuations
p'_{rms}, average	=	$(\sum_{i=1}^{N} p'\text{rms},i)/N$, where N is number of data points
p'_{rms} baseline	=	rms pressure fluctuation without control
Q''	=	instantaneous heat flux fluctuations
q'_{rms}	=	rms of heat flux fluctuations
Re_p	=	Reynolds number with respect to the primary airflow rate
r/R_0	=	normalized combustor radius
U_{sec}	=	mean axial velocity of the secondary stream
z	=	length along the combustor axis
ϕ	=	equivalence ratio

Introduction

COMBUSTION instabilities occur in a number of propulsion systems, such as jet engines, afterburners, and rocket engines. Unstable combustion induces large-amplitude pressure oscillations in the flow and can cause excessive noise, vibrations, and structural damage. In extreme cases, the oscillations can lead to a total loss of the flame. In recent years, emission regulations have come to demand operation near the lean blowoff limit, where combustion instabilities are a major problem. Rayleigh[1] was the first to define a criterion for thermoacoustic instability and observed that, if heat is added in phase with the oscillations, the pressure signatures are enhanced, whereas out-of-phase heat addition reduces pressure oscillations. The Rayleigh criterion has been extensively used in most analytical, computational, and experimental studies to characterize combustion instability.

Received 30 August 2001; revision received 4 June 2002; accepted for publication 1 July 2002.

*Professor, Mechanical Engineering Department. Member AIAA.
†Graduate Student, Mechanical Engineering Department.
‡Professor, Mechanical Engineering Department; currently Professor, Aerospace Engineering Department, University of Cincinnati, Cincinnati, OH. Member AIAA.

A considerable amount of work has been done on combustion control with gaseous fuels.[2–4] Richards and Janus[5] proposed a simple time-lag model and suggested that the thermoacoustic oscillations are a strong function of the nozzle velocity and geometry and that the oscillation amplitude scaled with pressure. Both active and passive control techniques have been used to suppress thermoacoustic instability. Passive control strategies usually involve geometrical redesign of an unstable combustor to reduce instability and pressure oscillations. As an example, Schadow et al.[6] have used multistep nozzles to break down the coherent structures through small-scale turbulent fluctuations induced by the multiple steps. However, passive control is specific to the combustor geometry and provides control over a limited operational range. On the other hand, active feedback control provides high performance over a wide range of operating conditions and provides a versatile approach toward extending the flammability limits and lowering emissions. In active control, an actuator is usually employed to provide the control authority. The pressure/heat release signals measured from the combustor are passed through a bandpass filter, and an appropriate phase shift and gain are introduced with respect to the sensor signals. The signal is then fed to the actuator to suppress the pressure oscillations.[2–4,7,8]

Recent reviews on active control of combustion instabilities can be found by McManus et al.[9] and Candel[10] Gutmark et al.[11–13] and Schadow et al.[14] have shown the effect of active shear layer excitation on the suppression of vortices, increased heat release in diffusion flames, and an extension of blowout limit in premixed flames. Yu et al.[7,8] have devised a control strategy utilizing periodic fuel injection, synchronized with large-scale structures to dampen unstable combustion oscillations. Lang et al.[2] applied the theory of antisound to construct a method for suppression of combustion instabilities. Bloxsidge et al.[3] have identified a vibrator that altered the blockage of flow as a potential actuator for control. The instability signal was phase shifted, amplified, and fed to the vibrator to produce fluctuating mass flow in the chamber. Gulati and Mani[4] used a similar gain/phase shift controller to suppress combustion instabilities. They pointed out the limited gain and phase margins of the controller in the presence of multiple modes using classical control techniques. McManus et al.[15] have used a pulse width modulation technique with an auxiliary fuel injector to dampen thermoacoustic instabilities. Neumeier and Zinn[16] and Neumeier et al.[17] used a wavelet technique to identify multiple modes in a combustor and to develop a gain/phase shift for each mode, which was used as a control input to the fuel injector to achieve control. Richards et al.[18,19]

have also used the concept of cyclical fuel injection for controlling instabilities.

A number of recent studies have been published where swirl-stabilized combustion has been specifically studied. Sivasegaram and Whitelaw[20] have studied the effects of swirl on combustion instabilities in different premixed combustor configurations. They have shown that swirl enhanced the instability for flames stabilized behind a sudden expansion and reduced the instability in disk stabilized premixed combustion. Stephens et al.[21] have investigated open-loop control in swirl-stabilized spray flames. They have demonstrated the potential improvements in heat release with airstream forcing. Paschereit et al.[22,23] identified the presence of unstable helical modes in a swirl-stabilized combustor and used a fuel equivalence ratio modulation strategy to reduce thermoacoustic oscillations. Cohen et al.[24] and Hibshman et al.[25] have used a self-tuning fuel modulation mechanism to suppress combustion instabilities in full-scale engine operation at realistic conditions.

The first objectives of the present paper are to explore the instability characteristics of a can-type, swirl-stabilized spray combustor and to explore active control strategies to suppress the thermoacoustic oscillations. Toward this end, a self-tuning feedback-loop controller has been implemented, and its ability to enhance the performance of the combustor has been examined. The majority of the studies on combustion instability have focused attention on pressure oscillations as the only measure of performance. An exception to this is the work of Sivasegaram and Whitelaw[26] and Sivasegaram et al.,[27] who explored the effect of control on NOx levels. However, their work was limited to that of premixed gaseous combustion. In this paper, attention is focused on nonpremixed, spray combustion, and the performance is characterized on the basis of pressure oscillations, as well as emissions levels.

The second objective of the paper is to report how control influences the mean velocity field and the turbulence levels. To this end, measurements of the velocity field are reported both with and without control. It is anticipated that because velocity fluctuations play a role in the acoustic–flame coupling, which, in turn, drives the combustion instability, control will likely influence the velocity field, and it is of interest to determine the level and nature of this influence. Whereas velocity measurements in spray combustors have been reported by many investigators,[28–33] none of these measurements have been made for a combustor operating in an unstable mode, and the effect of control on the velocity field has not been specifically reported. Providing such information is the motivation behind the second objective of the present work.

Experimental Setup

The experiments were performed in a model combustor (Fig. 1) operating at 30-kW heat release and atmospheric pressure. A Parker–Hannifin research simplex atomizer (RSA) nozzle is used to atomize the liquid fuel. Ethanol is used as the liquid fuel.

The combustor has provisions for two airstreams (Fig. 1). The RSA nozzle needs an airstream (the primary airstream) that is used to assist in the atomization of the fuel. The secondary airstream provides the bulk of the combustion air. The primary airstream is distributed in a circumferentially uniform manner to the combustion air chamber base by a manifold. A honeycomb is installed in the chamber to straighten the flow. The secondary airstream is distributed to the secondary inlets of the air chamber by another manifold. These inlets are uniformly arranged around the air chamber. The secondary air enters through two sets of swirlers, placed at two different axial locations around the nozzle barrel. Both airstreams enter the combustion chamber at standard temperature and pressure. The primary and secondary streams both have 45-deg swirl vanes, and the combustor was operated in a coswirl configuration. The swirl number based on the secondary flow swirler was estimated to be 0.8.

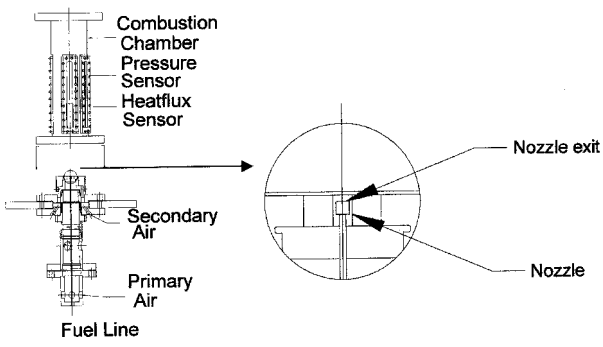

Fig. 1 Schematic of the combustor.

The liquid fuel is pressurized to 160 psi (N/m^2) in a fuel tank by high-pressure inert nitrogen, metered, and sent to the RSA nozzle through a tube mounted in the center of the air chamber. The RSA nozzle has a swirl chamber for the primary airstream and swirls the fuel/air mixture for improved atomization and dispersion. The Sauter mean diameter of the droplets generated at two-nozzle diameters downstream varied radially from 5 to 35 μm (Messina and Acharya[34]). The fuel stream was modulated using a valve (automotive fuel injector) driven by a signal processor or a function generator.

The average fuel flow rate was kept constant at 0.75 ml/s. The primary airflow velocity U_P of 2–110 m/s was delivered by a compressor operating at 20 atm. A pressure regulating valve reduced the line pressure to 5 atm upstream of the plenum feeding the combustor. Secondary air was introduced coaxially around the nozzle with a flow rate that varied from 0.283 to 1.7 m^3/s.

The combustion shell is 0.6 m in length and 0.14 m in diameter D. High-sensitivity, water-cooled pressure transducers (Kistler pressure transducer, Model 7061B) and heat flux sensors (Vatell Model HFM-6D/H) with frequency responses of 50 and 5 KHz, respectively, were mounted along the length and circumference of the combustor to measure the oscillations in the combustor for varying flow rates and fuel flow modulation frequencies. The pressure and heat flux sensors were collocated at the same heights along the length of the combustor at $z/D = 0.36$, 0.55, 0.73, 1.45, and 2.18. Two additional pairs of sensors were placed circumferentially at 90 and 180 deg at $z/D = 1.45$. Four high-temperature quartz glasses are mounted on the comubustor to provide optical access.

Controller Description

A schematic of the feedback control loop is shown in Fig. 2a. A high-speed microprocessor was used to perform real-time signal processing. The pressure and heat flux fluctuations, which were recorded from the high-sensitivity microsensors, were fed into the A/D converter of the I/O card present on a carrier board. The carrier board is linked through a digital signal processor (DSP) link 3 cable, which is a 32-bit, 40-Mbytes/s I/O interface to the Indy motherboard. The Indy motherboard holds a Texas Instrument 32-bit, 60-MHz microprocessor. The data are digitally filtered in blocks and phase shifted and amplified before being sent to the D/A converter. The signal to the D/A converter is further amplified to attain an optimum voltage (Fig. 2b), which is fed into a solid-state relay (Crydom Corporation Model DC60S7) powered by a battery to run the valve. Initially the fuel actuator frequency is matched with the instability

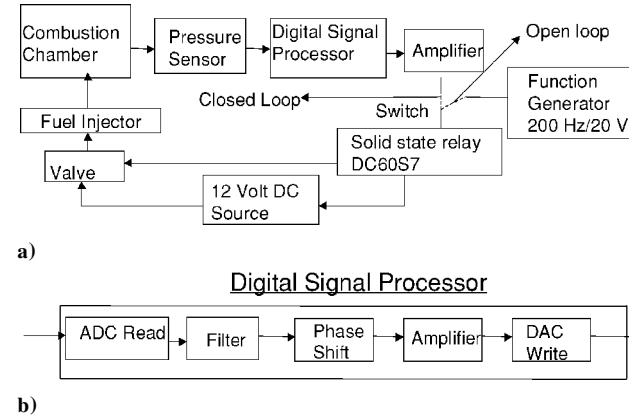

Fig. 2 Schematic of a) controller and b) DSP.

frequency, which is used as a driving signal for the valve. It is then switched to operate on the control signal once the first set of data is processed for every preset phase angle.

Velocity Diagnostics

A two-dimensional Dantec© fiberflow laser Doppler system operating in backscatter configuration was used to record the velocity of the reacting and nonreacting flow. Both the axial and tangential components were recorded. Although it was possible to record both components simultaneously using the control volumes generated by the blue and the green laser beams, measurements of the two components of velocity reported in this paper were performed separately in a one-dimensional mode with only the green beams. This was done because the power in the green beams was higher than in the blue beams and resulted in higher validation rates and signal-to-noise ratio. The probe was rotated by 90 deg to measure the second component of velocity.

The maximum systematic error (or fixed errors inherent in the laser Doppler velocimetry (LDV) system components) associated with these measurements is found to be 0.8%. For the reacting flow, the maximum precision error (or statistical errors resulting from finite sample populations) based on 5000 samples is less than 1.4% with a 95% confidence level at all axial locations. However, note that at many locations up to 10,000 samples were recorded, thus, reducing the precision error to 1%. Similarly, the maximum precision error at the 95% confidence level for the rms of the reacting flow velocities was less than 2% at all axial locations. At locations where 10,000 samples were recorded, the uncertainty is 1.4%. For the cold-flow condition, 3000 samples were recorded at each location yielding an uncertainty of 2 and 2.6%, respectively, for the mean and rms velocities at the 95% confidence level. These precision estimates were determined following guidance provided by Yanta et al.[35]

The mean velocity data were corrected for velocity bias using Dantec's residence time-weighting algorithm. This was done to eliminate the velocity bias toward higher velocities.

The reacting flowfield was seeded using 0.3-μm aluminum oxide particles. Although these particles are relatively expensive, they are

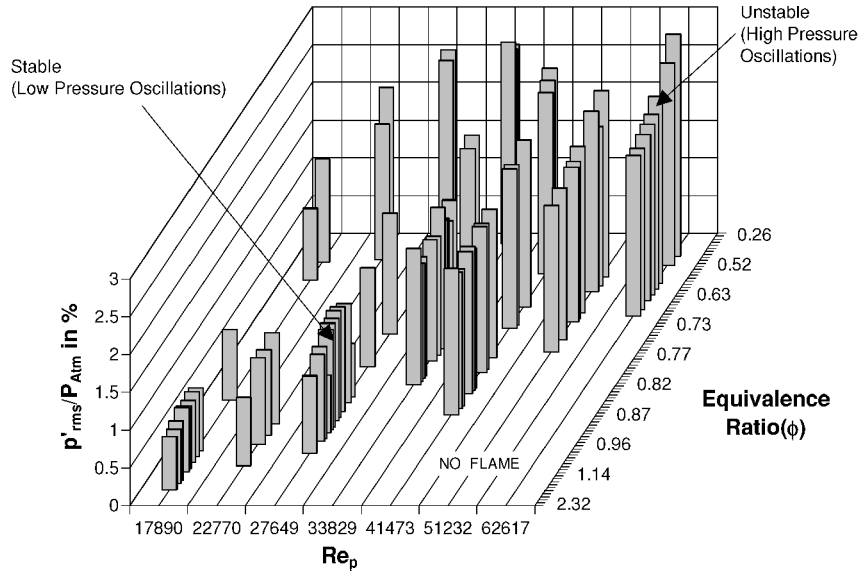

Fig. 3 Values of p'_{rms}/P_{atm} with swirl.

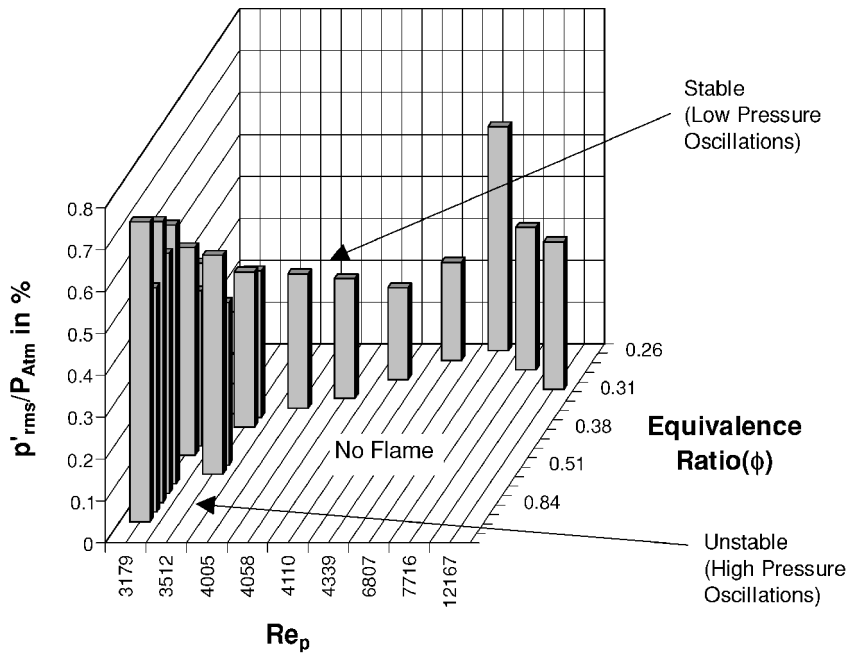

Fig. 4 Values of p'_{rms}/P_{atm} without swirl.

well suited for high-temperature environments due to their excellent thermal stability. In addition, these particles provide superior frequency response to the flow fluctuations. When the Kolmogorov timescale is used as the particle response time, it is estimated that the maximum particle diameter that will accurately represent the continuous phase is 0.9 μm. Thus, the particles used for the results presented here are sufficiently small.

Velocity measurements were also made of the cold, nonreacting flowfield, which was seeded using smoke particles. Rosco® fog fluid that was heated in a separate vessel outside the combustion chamber generated the smoke. The smoke was then removed from the liquid surface inside the vessel and injected into the combustion chamber via the secondary air ports.

Results and Discussion

Characteristics of the Combustor

To characterize the behavior of the combustor, pressure measurements were made for a range of equivalence ratios and primary-airflow rates. The root mean square of the pressure fluctuations p'_{rms} can be used as a measure of the combustion instability in the combustor. The p'_{rms} values, normalized by the mean combustor pressure (1 atm) and expressed as a percentage, are presented as a function of the equivalence ratio ϕ and the primary-airflow rate represented by a Reynolds number $Re_p = U_p D/\mu$. Figure 3 shows the $p'_{\text{rms}}/P_{\text{atm}}$ values for a range of flow conditions for which a flame was obtained. It is evident that both the equivalence ratio and the primary-air Reynolds number influence the flame stability and the amplitude of the pressure oscillations. Highest pressure oscillations were observed at low equivalence ratios and high primary-air Reynolds numbers. As the equivalence ratio reaches the lean flammability limits, the propensity for oscillations increases, and the amplitude of the pressure oscillations are expectedly high. As the equivalence ratio increases, the flame is expectedly more stable, and the oscillation amplitudes are lower. There was roughly a 32% increase in pressure fluctuations for a 50% decrease in equivalence ratio at $Re_p = 6.2617 \times 10^4$. However, there is lower limit of equivalence ratio equal to 0.26 (close to the mean flammability limit) beyond which the flame is extinguished. This limit increases as Reynolds number Re_p increases. Note that as Reynolds number Re_p increases, the residence time of the fuel droplets in the flame zone is reduced, and hence, burning can not be sustained for very rich fuel/air mixtures. At low primary-air Reynolds number, the droplet residence times are long, and a flame can be stabilized for equivalence ratios in excess of two. However, under these conditions the flame is sooty and elongated due to insufficient air for combustion. In addition, at higher equivalence ratios, CO emissions increased indicating incomplete combustion.

Figure 4 shows the combustor pressure fluctuations without the swirl vanes (zero swirl). Because the recirculating toroidal region does not exist without the swirl vanes, there is no strong stabilization mechanism present, and the range of operating conditions is very limited. A stable flame could be obtained at low Reynolds number Re_p or low equivalence ratios. As the primary-air Reynolds number increased, the flame was lifted until it ultimately blew off.

For the swirl-stabilized situation, a number of flow conditions were selected, which were representative of both high $p'_{\text{rms}}/P_{\text{atm}}$ (nearly 3%) and low $p'_{\text{rms}}/P_{\text{atm}}$ (nearly 1%). High $p'_{\text{rms}}/P_{\text{atm}}$ (2–3%) corresponds to elevated combustor noise levels and low $p'_{\text{rms}}/P_{\text{atm}}$ (less than 1%) corresponds to smooth combustion. The high-pressure oscillation case corresponded to a $Re_p = 6.1626 \times 10^4$ and $\phi = 0.429$ and had relatively low NOx levels, whereas the low-pressure oscillation case corresponded to a $Re_p = 6.1473 \times 10^4$ and $\phi = 0.609$ and had relatively high NOx levels. The higher NOx levels at $\phi = 0.609$ are due to the higher equivalence ratio associated with this case. Measurements of the temperature, CO, CO_2, and NOx were made at the midpoint of the combustor exit with an Enerac 3000 emission sensor. The velocity measurements (with and without control) were made for conditions close to those of the high-pressure oscillation case, where the normalized pressure oscillations were in the vicinity of 2.5%.

Figures 5a–5d present the stack emission and temperature data for different $p'_{\text{rms}}/P_{\text{atm}}$ levels representing different flow conditions

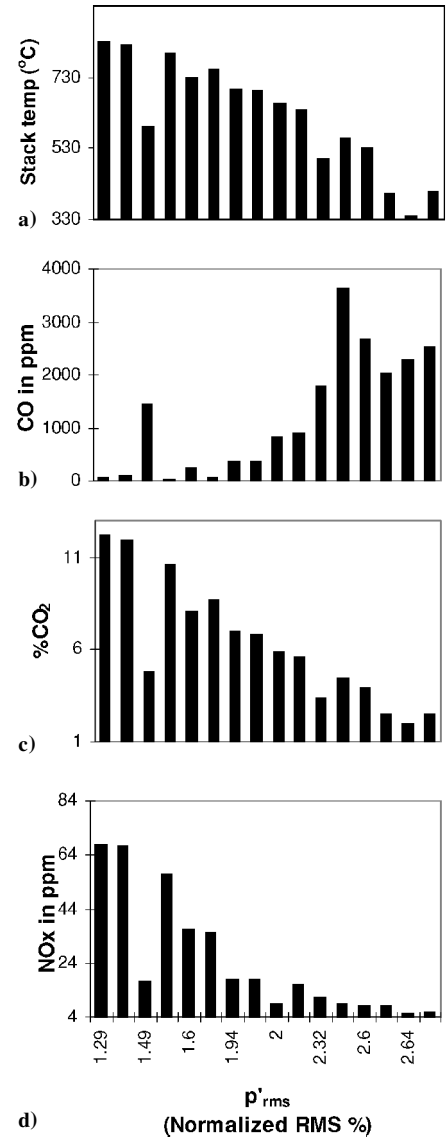

Fig. 5 Different $p'_{\text{rms}}/P_{\text{atm}}$ conditions (and different equivalence ratio conditions) at centerpoint of the combustor exit: a) temperature and b–d) emissions.

(different equivalence ratios). As the $p'_{\text{rms}}/P_{\text{atm}}$ is increased [associated with lower equivalence ratios (Fig. 3)], the temperatures and NOx levels decrease, while CO increases and CO_2 levels are correspondingly reduced. Exhaust stack temperatures were nearly 200% higher at the lower CO levels, while the corresponding change in NOx levels were as high as 60 ppm at 4.5% O_2 concentration. Lower centerline stack temperatures (and NOx) at the higher oscillations suggest the possibility of incomplete combustion and explain the observed higher CO and lower CO_2 levels.

Note that centerline stack data are local point measurements and should not be directly correlated with pressure oscillations in the combustor; rather, the radial profile at the exhaust should be considered. Whereas increasing pressure oscillations is related to decreasing equivalence ratios (and lower NOx and temperatures), it is not the only controlling factor because the aerodynamic effects associated with Reynolds number Re_p play an important role, as seen earlier in Figs. 3 and 4. Further discussion attempting to correlate the emission data (centerline and stack averaged) with the p'_{rms} and q'_{rms} fluctuations is presented later.

To further understand the nature of the instability in the swirl-stabilized flame, the pressure and heat flux signatures were analyzed in the frequency domain. The heat flux sensors measure the convective and radiative heat flux to the wall, which is expected to

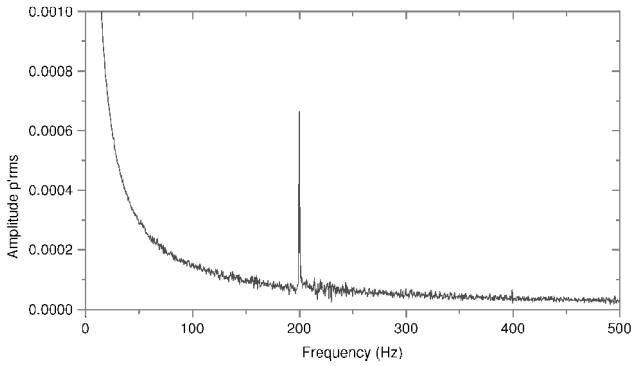

Fig. 6 Values of $p'_{\rm rms}$ (arbitrary units) spectra at $\phi = 0.429$ and $Re_p = 6.1626 \times 10^4$.

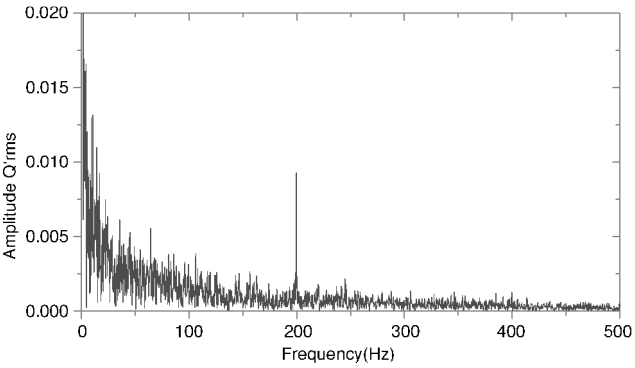

Fig. 7 Values of $q'_{\rm rms}$ (arbitrary units) spectra at $\phi = 0.429$ and $Re_p = 6.1626 \times 10^4$.

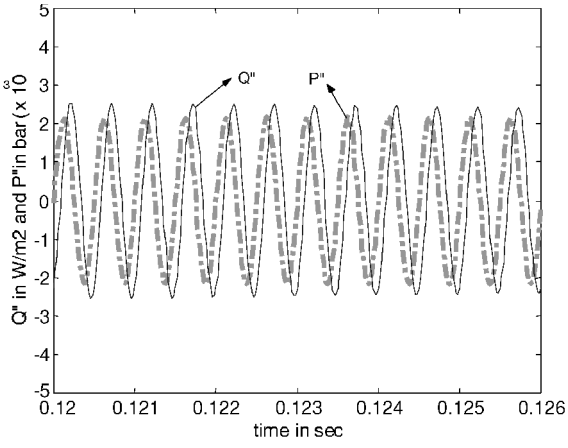

Fig. 8a Pressure and heat flux time trace recorded at $z/D = 0.36$.

be proportional to the heat release in the flame. Figures 6 and 7 show amplitude spectra of the pressure and heat flux corresponding to an unstable condition ($\phi = 0.43$ and $Re_p = 6.2616 \times 10^4$). Both spectra show a single dominant peak at 200 Hz. The pressure and heat flux data are plotted on the same timescale in Fig. 8a. These data were taken at $z/D = 0.36$. Intermittent behavior was noticed where the P'' and Q'' were in phase at most instances of time and out of phase at other instances. A local Rayleigh index was computed for the described case (Fig. 8b) by computing the product P'' and Q''. This index was greater than zero for most of the time, and this was sufficient to sustain the fundamental oscillation originally excited by the flame. Thus, the pressure and heat flux oscillations are coupled with each other, driving the combustor into thermoacoustic resonance.

The thermoacoustic instability at 200 Hz was identified to correspond to a longitudinal quarter-wave mode instability in the combustor shell. This conclusion was based on performing a cross cor-

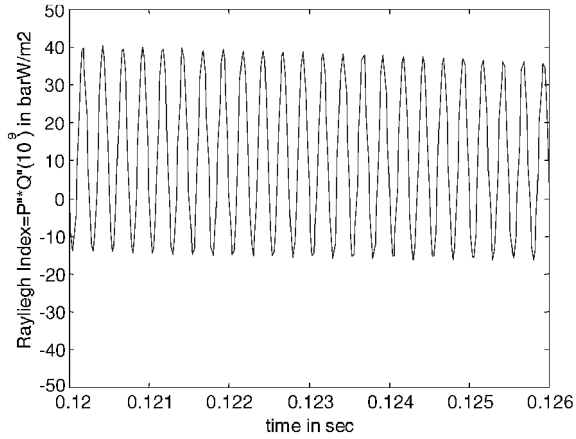

Fig. 8b Corresponding Rayleigh index for $\phi = 0.429$ and $Re_p = 6.1626 \times 10^4$.

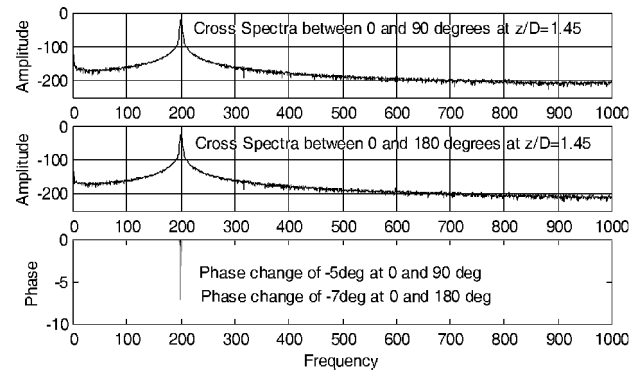

Fig. 9 Cross spectra for sensor signals at different circumfrential locations.

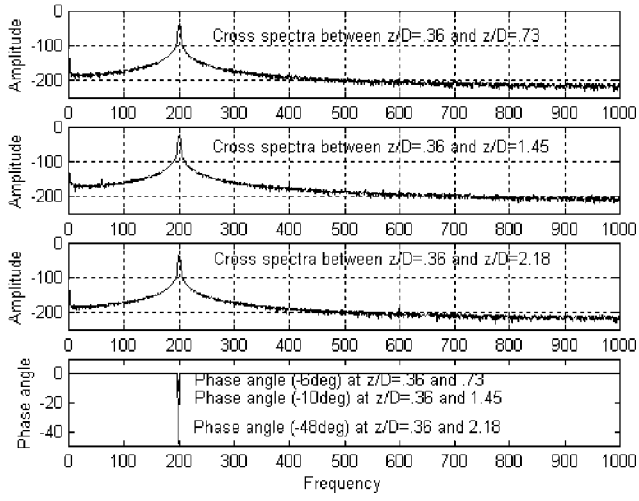

Fig. 10 Cross spectra for sensor signals at different longitudinal locations.

relation between different sensor signatures located along the longitudinal axis and between the sensors located at different angles along the circumference of the combustor. This cross spectrum in the circumferential direction is shown in Fig. 9 and in the longitudinal direction, as shown in Fig. 10. The amplitudes in the cross-spectrum plots clearly indicate the presence of a strong instability at 200 Hz. The phase plots in Figs. 9 and 10 obtained by a correlation of pressure–time signal at 0, 90 and 0, 180 deg around the circumference reveals a phase change of less than 7 deg. This implies that the azimuthal and radial instability were not excited. A phase change was observed in the cross spectrum obtained from

the axially located sensors. The cross spectra computed between the sensor signals at $z/D = 0.73$, 1.45, and 2.18 indicate a phase change of -6, -10, and -48 deg, respectively. Because the combustion chamber length is $z/D = 2.66$ and the last sensor was located at $z/D = 2.18$, it is believed that the pressure node is located farther downstream from the sensor. This implies that there could be an additional phase change that would result farther downstream toward the exit of the combustor. These observations point to the presence of a quarter-wave mode instability.

To further support the existence of the quarter-wave mode, an estimate of this frequency was calculated using $f_{1/4} = c/4L$, where c is the speed of sound and L is the length of the combustor. The estimated frequency is 256 Hz and is slightly larger than the measured instability frequency. This discrepancy can be explained by two unrealistic assumptions in our frequency estimation. First, the open end/exhaust is considered as a pressure, node but it has been shown by Bracco[36] that the pressure node is always located downstream of the exhaust section. This leads to overestimation of the acoustic eigenfrequencies. Second, the temperature field is nonuniform in a turbulent reacting flowfield. Ando[37] has numerically studied the effect of nonuniformities of one-dimensional temperature fields on the frequency of standing acoustic waves. His analysis indicates that axial temperature nonuniformity can lower the frequency of the acoustic standing wave by as much as 20%. Thus, it is seen that properly estimating these parameters would lead to a frequency estimate of the quarter-wave mode to be closer to the measured instability frequency.

Open-Loop Control

Open-loop control experiments were done under the premise that the fuel/air mixing could be beneficially impacted by controlling the frequency with which the fuel is injected into the combustor. This frequency will effect the heat release dynamics which, in turn, will control the thermoacoustic coupling and the associated instability. The heat release dynamics can also influence the emissions.

Conditions that correspond to a high level of NOx ($\phi = 0.609$ and $Re_p = 4.1473 \times 10^4$) were chosen for open-loop control. For this baseline condition, NOx levels of 60 ppm were obtained. The frequency response of the combustion oscillations were determined by pulsing the valve with an average flow rate of 0.75 ml/s at 160 psi between 30 and 340 Hz with a sinusoidal signal. The signal was generated by a function generator, 10 V peak to peak, with an arbitrary phase and sent to a solid-state relay, which was powered by a battery to run the fuel actuator. Simultaneous NOx, CO, stack temperature, and O_2 were recorded from the Enerac 3000 emission sensor located in the center at the open end/exhaust of the combustor. The $p'_{\rm rms}$ along with the corresponding unstable frequencies were recorded for different excitation frequencies. These results are presented in Fig. 11 and are normalized by the average value over the entire range of excitation frequencies.

Figure 11a shows the presence primarily of an oscillation peak centered at about 220 Hz. There is a ±40-Hz spectral broadening around the 220-Hz peak. As noted earlier, this peak corresponds to a quarter-wave mode, and the oscillations were amplified or reinforced by forcing at the instability frequency. A secondary peak (not shown) was also noticed around 310 Hz. At frequencies greater than 330 Hz, the flame could not be sustained. Figures 11b–11e represent the centerline stack emissions at different forcing frequencies. The highest centerline exhaust temperature was obtained in the range of 170–220 Hz and correlated well with the highest NOx, highest CO_2, and lowest CO. The 170-Hz frequency corresponds to the beginning of increased pressure oscillations, whereas the pressure oscillations peak at 220 Hz. The correspondence between high-pressure oscillations and NOx was also observed by Sivasegaram and Whitelaw[26] and Sivasegaram et al.[27] in their studies of premixed gaseous combustion. At 220 Hz, corresponding to the highest pressure oscillations, a reduction of 70% CO (relative to the average) was observed. Between 130 and 160 Hz, pressure oscillations were low, but high levels of CO was observed, and the flame was essentially sooty, indicating inefficient burning at these lower frequencies.

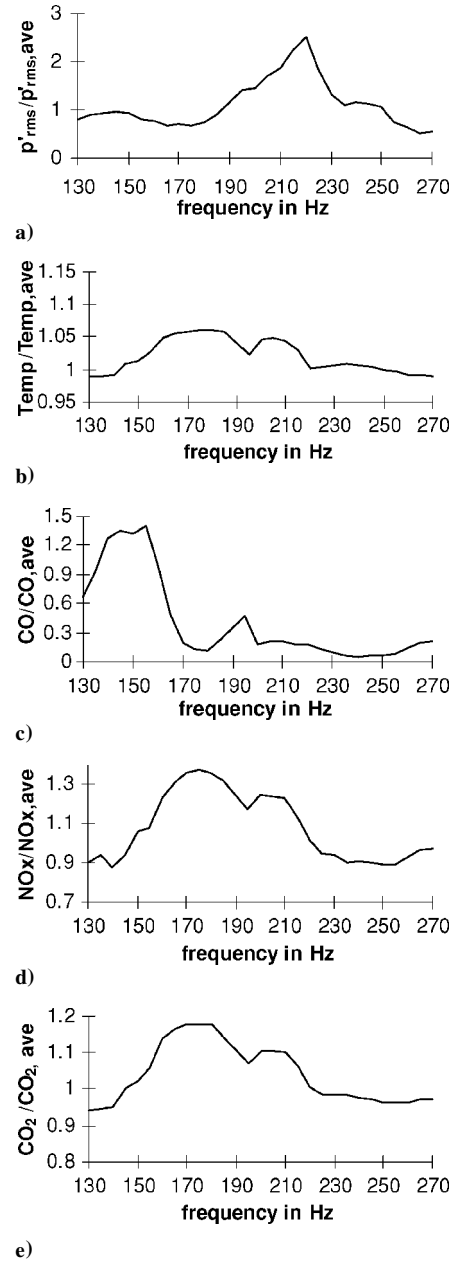

Fig. 11 Pressure fluctuations, temperature, and emissions vs frequency (open loop).

Closed-Loop Control

A closed-loop feedback control system was designed to suppress levels of pressure and heat release oscillations in the combustor at unstable conditions. The control strategy is driven by Rayleigh's criterion and is based on the premise that if the heat release dynamics is out of phase with the pressure oscillations, thermoacoustic coupling will not result. The heat release dynamics is controlled by the frequency and phase of the signal used to drive the automotive fuel injector valve.

The signal used to drive the fuel injector valve is obtained from the Kistler pressure transducer (pressure signature), which is sent to a digital signal processor, where it is filtered to remove the low-frequency noise, amplified, and phase shifted. The phase shifting is the key driver for decoupling the heat release dynamics from the acoustics in the combustion chamber. The signal written to the D/A converter is further magnified to reach an optimum voltage. This signal is then sent to the fuel-injector valve. The phase delay was varied between 0 and 360 deg between the sensor and control signature. Different phase delays were examined because the optimum phase corresponding to maximum suppression can not be determined

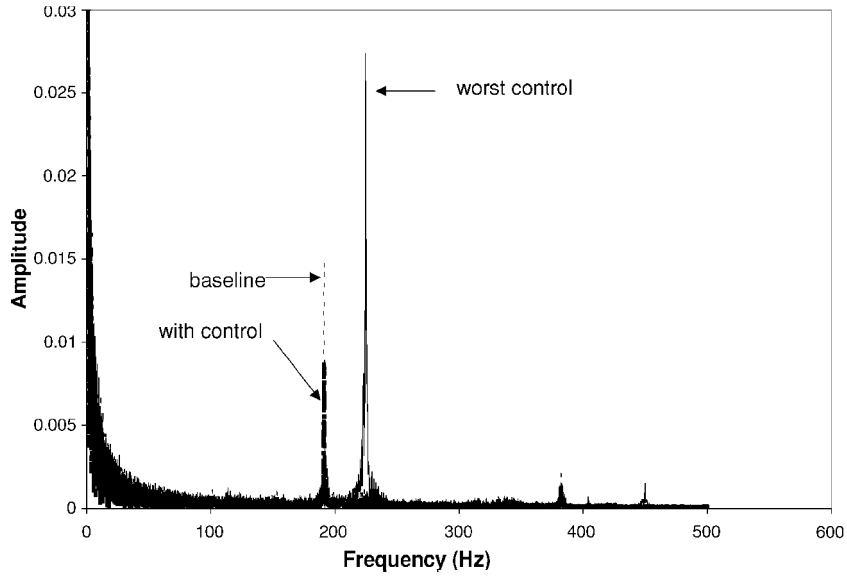

Fig. 12 Amplitude of the pressure spectra (arbitrary units) baseline, best, and worst control.

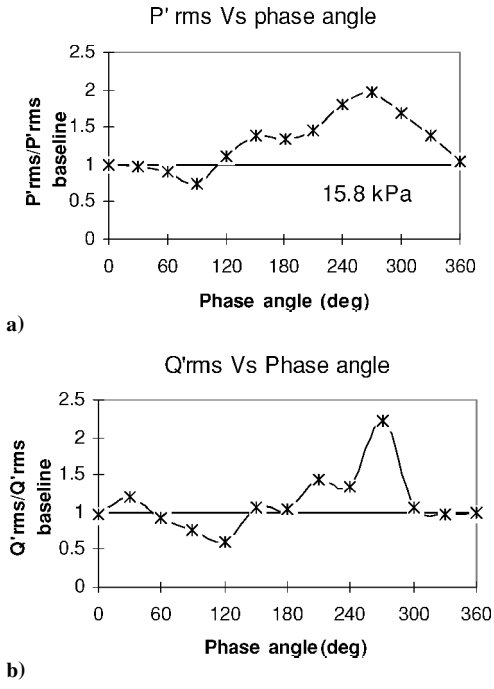

Fig. 13 Closed-loop control: a) Normalized $p'_{\rm rms}$ vs phase angle and b) Normalized $q'_{\rm rms}$ vs phase angle.

a priori due to the intrinsic delays involved in the system, such as the fuel/air mixing, fuel convection, ignition, and flame propagation.

Two sets of conditions were chosen for active control. The first set involves a flow condition for low-pressure fluctuation but high levels of NOx ($\phi = 0.609$ and $Re_p = 4.1473 \times 10^4$). The second condition involves high-pressure oscillation levels, but relatively lower NOx levels ($\phi = 0.429$ and $Re_p = 6.1626 \times 10^4$). The pressure, heat release, and emissions were all simultaneously recorded under the controlled conditions for different preset phase-delay values.

Figures 12–14 show the effect of closed-loop control for the first baseline case corresponding to high NOx levels (60 ppm). Figure 12 shows the amplitude pressure spectra for the baseline and phase-delay conditions representing the worst and best control. Best control, where the largest reduction in pressure oscillations is obtained, was achieved around 90-deg phase delay. As noted earlier, due to time delays introduced by droplet convection, evaporation, and mixing, the optimum phase delay for control is not 180 deg. The worst control, where pressure oscillations are amplified, was obtained at around 270-deg phase delay. It was noticed that at worst control the peak in the oscillation frequency was located around 225 Hz, whereas for the baseline and best control the peak frequency was at 200 Hz. The change in the peak frequency may result from the differences in the fuel mixing (because the phase of fuel injection is different), which can influence the temperatures (and, thus, the acoustics), as well as the heat release dynamics.

As shown in Fig. 13, the most suppression of oscillations was achieved at 60–120 deg phase angle delay. For the best control conditions, at 90-deg phase delay, the $p'_{\rm rms}$ and $q'_{\rm rms}$ fluctuations dropped by 30 and 40%, respectively (Figs. 13a and 13b). These reductions are relatively modest and considerably lower than the reductions achieved for the second set of flow conditions corresponding to the high-pressure oscillation case. However, a 40% reduction in NOx levels was achieved for 0–120 deg phase delay (Fig. 14c), with only a 4% reduction in the temperature (Fig. 14a) at 60-deg phase delay, where optimal control was achieved. As noted earlier, this observed correlation between a reduction in the pressure oscillations and the NOx level is consistent with premixed gaseous combustion studies of Sivasegaram and Whitelaw[26] and Sivasegaram et al.[27] The 60-deg phase delay is also associated with a 10% reduction in CO_2 and a 30% increase in CO.

The 30% reduction in the pressure levels combined with a 40% reduction in NOx for the best control condition are quite encouraging, particularly in view of only a 5% reduction in temperature. This indicates improved radial mixing between the fuel and air and reduction in the peak equivalence ratio, NOx, and temperature. However, as noted earlier in Fig. 5, the pressure oscillations measured along the combustor walls may not correctly correlate with the centerline stack measurements, but may correlate better with the an average measurement across the exit cross section. To investigate this, measurements were made at three radial locations across the combustor exit plane for the baseline and the best control cases. These measurements are shown in Figs. 15a and 15b and indicate that, with best control, more uniform temperature distributions and lower NOx were indeed obtained across the entire cross section of the combustor. This implies that control provides dual benefits of reducing pressure oscillations and, at the same time, improving radial mixing leading to lower NOx and more uniform temperature distributions.

The effect of feedback-loop control for the high-pressure fluctuation condition (baseline $p'_{\rm rms} = 2.93\%$) is shown in Figs. 16–18. The baseline Case in Figs. 16–18 corresponds to $\phi = 0.429$ and $Re_p = 6.1626 \times 10^4$. Best control is achieved at 60-deg phase delay (Figs. 17a and 17b), and the amplitude of the 200-Hz oscillations is reduced by a factor greater than three (Fig. 16). However, this substantial suppression of the 200-Hz oscillation is accompanied by the

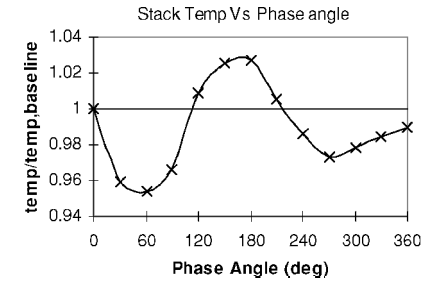

a)

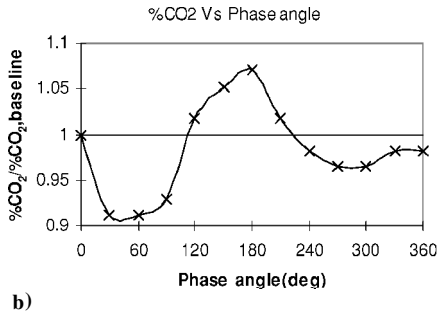

b)

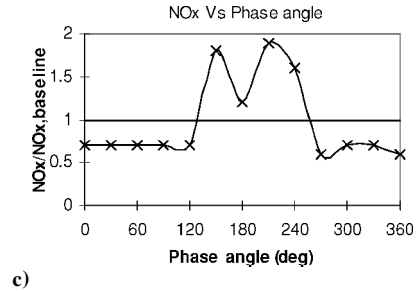

c)

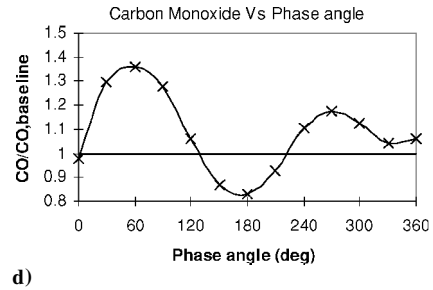

d)

Fig. 14 Emissions vs phase angle (closed loop): a) stack temperature vs phase angle, b) %CO_2 vs phase angle, c) NOx vs phase angle, and d) carbon monoxide vs phase angle.

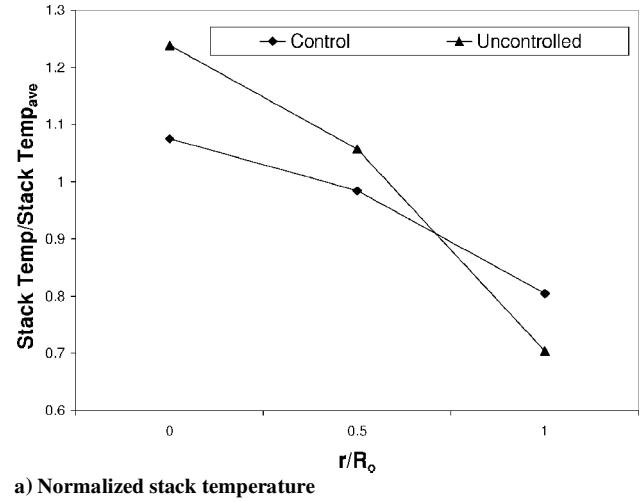

a) Normalized stack temperature

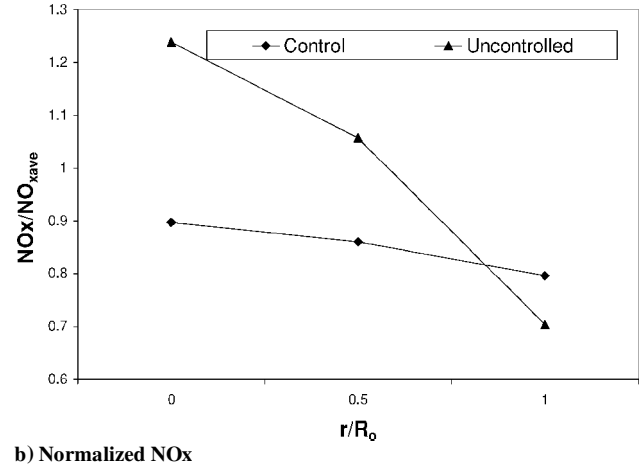

b) Normalized NOx

Fig. 15 Three different radial locations.

emergence of a secondary mode at 230 Hz with roughly the same energy as the 200-Hz mode. The net effect of the 60-deg phase-delay control is that the p'_{rms} and q'_{rms} decrease by 50 and 40%, respectively (Figs. 17a and 17b). For this optimal phase-delay condition, centerline exit temperature levels are slightly enchanced, and NOx, CO, and CO_2 levels are unaffected. This indicates that control with the correct phase delay is effective in reducing oscillations without adversely effecting the emissions. NOx reductions in the range of 15–20%, with associated increases in CO by 20–40%, are seen for phase delays between 0–60 and 180–270 deg. The temperature variations, though small (less than 6%), are consistent with the centerline emissions, decreasing with decreasing NOx and increasing CO. However, the heat flux fluctuations do not show a consistent correlation with temperature, which confirms once again that data from a wall-mounted sensor can not be directly correlated with the centerline exit data and that radial variations in the exit plane profile must be considered.

To further investigate the relationships between wall-mounted pressure and heat flux sensors (p'_{rms} and q'_{rms}) and stack conditions, stack measurements were obtained at different radial and circumferential locations and then averaged. It is expected that measurements averaged over the exit plane are better correlated with the pressure oscillations than the centerline stack measurements shown earlier. These measurements were done for slightly different flow rate conditions than the high p'_{rms} case, but the general conclusions made here should apply to the two cases presented earlier. Measurements were made for three conditions: open loop, which represents the baseline case with strong pressure oscillations; best control (with 90-deg phase delay), where pressure oscillations were reduced by nearly 40%; and worst control (with 240-deg phase delay), where pressure oscillations were enhanced by nearly 95%. Table 1 shows that, with best control (lowest pressure oscillation), lower average CO (about 23%) and NOx levels (about 12%), associated with lower temperatures, were achieved in comparison to the open-loop baseline case. This observation is encouraging because pressure reductions are achieved together with a reduction of emissions. In worst control, the pressure oscillations are stronger than the open-loop baseline and lead to higher periodic heat release contributing to higher CO_2. Higher temperatures were also noticed, which corresponded to nearly 10% higher NOx. The CO emissions were relatively unaffected with worst control. Note that, in Table 1, the heat flux measurements along the wall are consistent with the stack-averaged temperature measurement, whereas in Fig. 18, as noted earlier, inconsistencies were noted between the centerline stack measurements and the wall heat flux. This confirms the earlier speculation about the importance of the radial variations at the combustor exit plane and the importance of incorporating these variations in any correlation with wall-mounted data.

Velocity Measurements

Figure 19 shows the mean axial velocity profiles along the radial direction for four axial locations along the length of the combustor.

Table 1 Effect of control on average emissions

Condition	Normalized p'_{rms}	Normalized q'_{rms}	CO, ppm	NOx, ppm	% O_2	% CO_2	Stack temperature, °C
Open loop	1	1	2578	16.38	14.65	3.95	448.37
Best control	0.61	0.52	1966	14.33	16.31	3.4	327.58
Worst control	1.95	1.85	2585	18.125	15.69	4.7	461.57

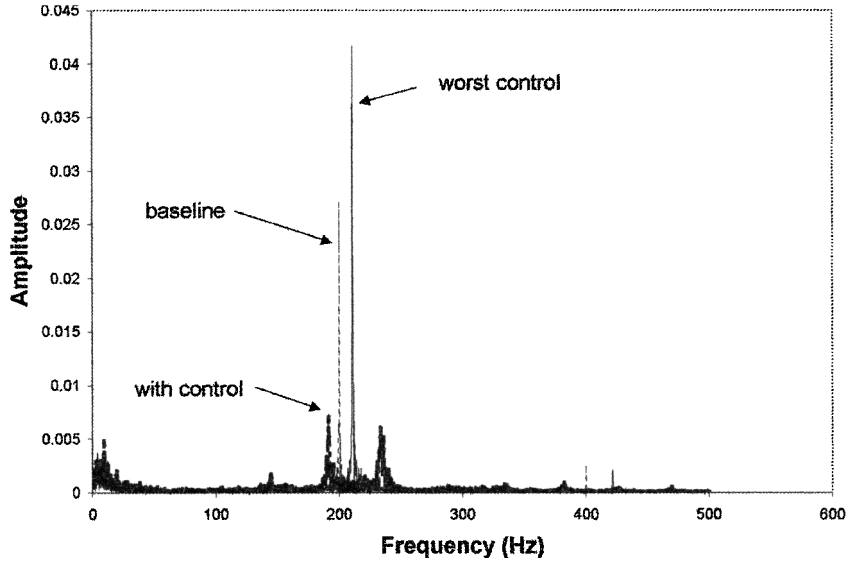

Fig. 16 Amplitude of the pressure spectra (arbitrary units) baseline, best and worst control.

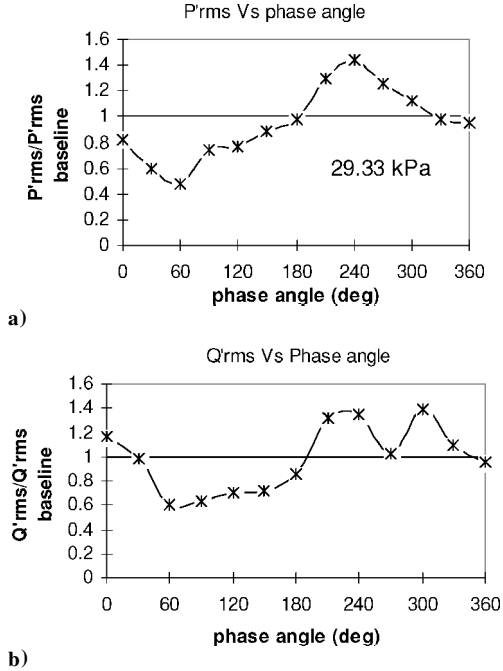

Fig. 17 Values of a) p'_{rms} vs phase angle and b) q'_{rms} vs phase angle.

Data are shown at axial locations of 0.256, 0.398, 0.540, and 0.682 shell radii above the nozzle. The velocities for both the controlled and uncontrolled reacting flow conditions are plotted together in Figs.19. The radial location of the secondary air swirler is shown. The reacting flow velocities were normalized by their respective mean inlet axial velocities of the swirling secondary airflow.

The flowfield for the uncontrolled condition is characterized by a central recirculation region (negative velocities) and a jet or shear-layer-type region (with large velocity gradients). The recirculation region is fairly large and develops rapidly in the radial direction with increasing streamwise distance. At $z/R_0 = 0.256$, the velocity profile becomes negative at $r/R_0 = 0.25$. (See Fig. 20, where the width of the negative velocity region is plotted.) At farther downstream locations, the negative velocities begin to appear increasingly closer to the shell. At $z/R_0 = 0.967$ (not shown), the negatives velocities appear as close to the shell as $r/R_0 = 0.7$. Beyond $z/R_0 = 0.967$, the recirculation region begins to shrink toward the centerline. In the jet region, the peak velocities move progressively outward downstream of the nozzle exit. At $z/R_0 = 0.256$, a peak nondimensional velocity of 1.38 occurs at $r/R_0 = 0.534$. However, this peak velocity spreads quickly in the radial direction and at $z/R_0 = 0.825$ reaches a magnitude of 1.29 at $r/R_0 = 0.833$.

The control condition exhibits similar radial spreading of peak velocities and growth of the recirculation zone. However, comparing the controlled and uncontrolled conditions reveals that the control has a significant effect on the flowfield. Examining the first four axial positions shows that with control there is a decrease in the magnitude of the peak velocity outside the recirculation region. This is accompanied by a modest decrease in the width of the recirculation zone at $z/R_0 = 0.256$ and 0.398 (shown in Fig. 20). However, by $z/R_0 = 0.540$, the recirculation regions for both cases have nearly identical radial extent. Of particular importance is that the velocity magnitudes in the recirculation region were enhanced significantly for the controlled condition. Comparing the magnitude of the maximum velocity in the recirculation region for each condition reveals a 20, 25, and 50% increase with control at $z/R_0 = 0.256$, 0.398, and 0.540, respectively. This enhancement of the recirculation zone in the near field is associated with a more stable combustor operation because the recirculation acts as a continuous ignition source through the entrainment of hot gases from downstream locations. Note that the heat release dynamics is often associated with the dynamics or breakdown of the central vortex. In such cases, improved stabilization of the central recirculation can be correlated with control of the instability.

Figure 19 also distinguishes those radial locations where no seeding was used to obtain velocity measurements (shown by solid symbols). Seeding was not used at these locations because increased seeding concentrations did not provide any increase in data rates.

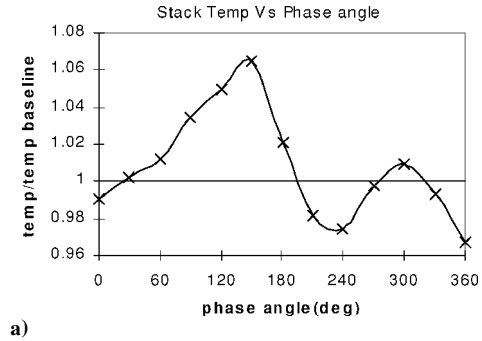

a)

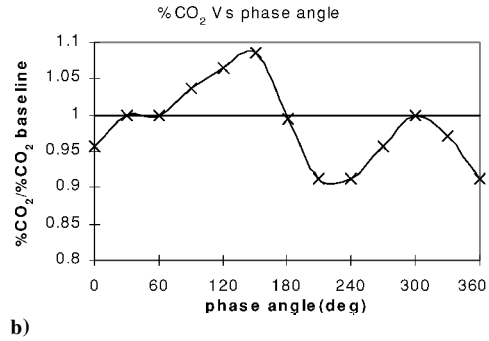

b)

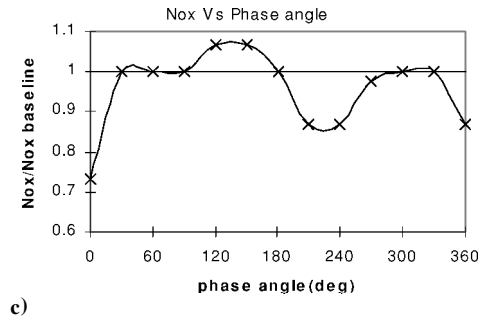

c)

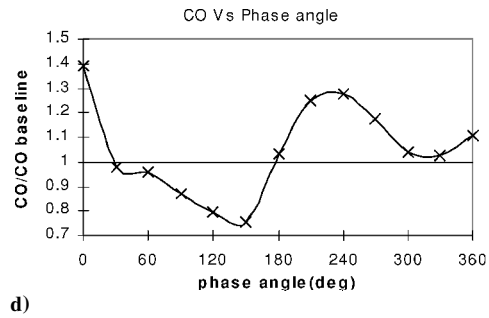

d)

Fig. 18 Emissions vs phase angle (closed loop): a) stack temperature vs phase angle, b) %CO_2 vs phase angle, c) NOx vs phase angle, and d) CO vs phase angle.

Therefore, the velocity distributions measured at these locations are composed entirely of unburnt droplets. For both the controlled and uncontrolled conditions, the radial locations of all unburnt droplets were outside the recirculation zone at every axial location. It is suspected that the velocity distributions at these locations are composed mostly of the larger diameter droplets. These droplets have increased momentum and inertia and, therefore, are not entrained into the recirculation region. At $z/R_0 = 1.393$ (data not shown) unburnt droplets were no longer detected, which indicates that all of the droplets were finally vaporized and had undergone combustion.

Figure 20 shows a measure of the shear layer width (defined here as the radial distance between the location of u_{maximum} and $\frac{1}{2}u_{\text{maximum}}$) and the growth of the recirculation zone downstream of the nozzle. Both reacting-flow and cold-flow data (under replicate flow conditions) have been included in Fig. 20. The reacting-flow cases exhibit an initial decay (up to $z/R_0 = 0.682$) in the measure of the shear

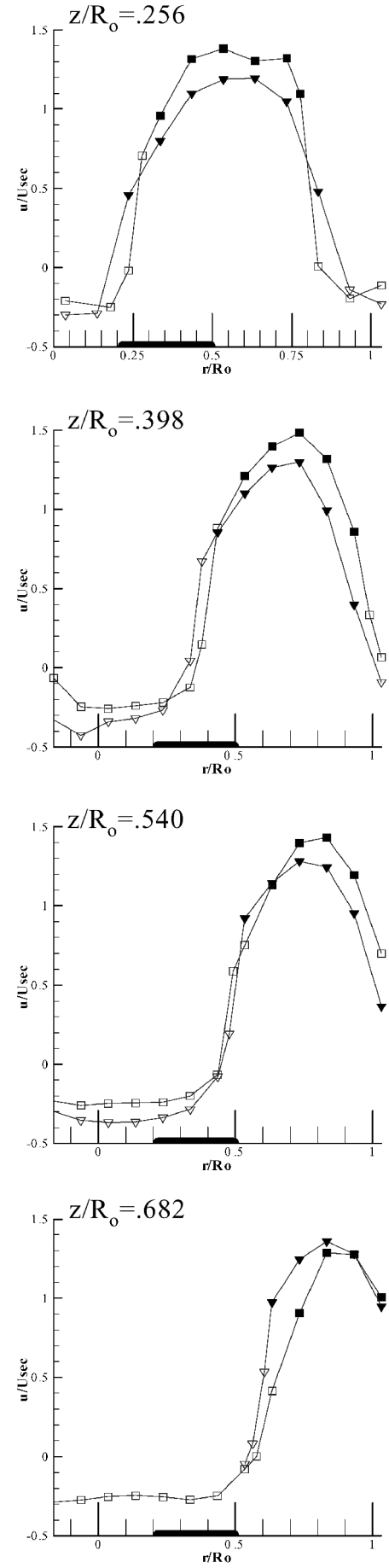

Fig. 19 Mean axial velocity for reacting flow U_{sec} = 11 m/s, secondary airflow velocity: solid symbols, no seeding; ■, no control and ▼, control.

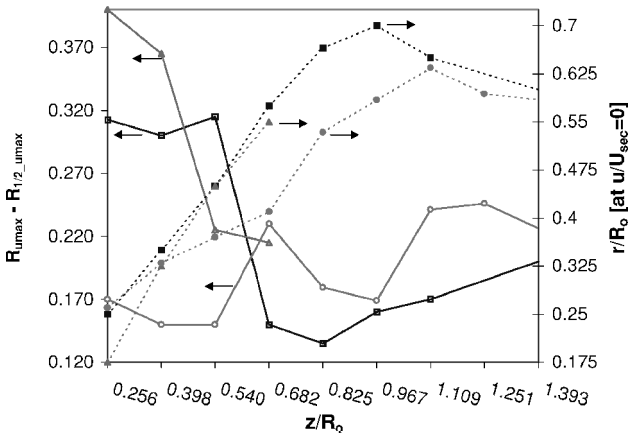

Fig. 20 Radial spreading of mean axial velocity downstream of RSA exit: left *y* axis, radial spreading parameter; right *y* axis, width of recirculation zone; $R_{u\,\max}$, nondimensional location of maximum axial velocity; $R_{1/2\,\max}$, nondimensional location of half of the maximum axial velocity; solid symbols, no seeding; ■, no control; ▼, control; and ●, cold flow.

layer width. This decay arises because the width of the recirculation region grows radially downstream of the nozzle, whereas the location of maximum velocity spreads radially outward at a slower rate. However, farther downstream, the jet spreading increases for the uncontrolled condition as the recirculation region shrinks. In the near field, the spreading of the shear layer for the controlled condition is much greater than for the uncontrolled condition and indicates greater entrainment and near-field mixing. These factors also contribute to the improved stability for the controlled condition.

The shear layer width for the cold-flow condition shows relatively modest variations (compared to the reacting-flow cases) up to $z/R_0 = 0.967$. It exhibits an increase at the next two axial locations and then begins to decay at $z/R_0 = 1.393$. In addition, the cold-flow condition has a smaller radial extent of the outer recirculation region in comparison to the reacting-flow condition at nearly all axial locations up to $z/R_0 = 1.109$ (the only exception being at $z/R_0 = 0.256$).

The axial rms velocity fluctuations are shown in Fig. 21. Based on these rms profiles, it is evident the sharp gradients in the shear layer regions observed in the mean axial velocity profiles are characterized by high-turbulence levels. Active control reduces not only the pressure oscillations but also the axial velocity fluctuations. Because pressure gradients drive the flow, the correlation between the pressure and velocity fluctuations are not unexpected. The strong velocity fluctuations may be manifested either via system–feed coupling in the combustor or by vortex shedding, leading to the heat release dynamics associated with the thermoacoustic instability.

Consider the axial rms velocity fluctuations for the reacting flow at $z/R_0 = 0.256$. The sharp gradients revealed in the mean axial profiles, which also correspond to inflection points between the inner recirculation zone and outer shear layer region, occur at $r/R_0 = 0.24$ for the control condition and $r/R_0 = 0.28$ for the uncontrolled condition. As expected, the axial fluctuations are also strongest near this radial position, reaching a maximum nondimensional value of 0.5 and 0.54 for the controlled and uncontrolled conditions, respectively. At $z/R_0 = 0.540$, the peak gradient in the mean axial velocity for both conditions occurs at $r/R_0 = 0.48$. This radial location corresponds precisely with the peak fluctuations of 0.455 and 0.464 for the controlled and uncontrolled conditions. This behavior is exhibited up to $z/R_0 = 0.825$. These sharp gradients in the mean velocity profiles are the locations where the production in the turbulence kinetic energy peaks and are attributed to the strong interactions between unburned droplets and hot recirculating gases. These strong interactions result in the large fluctuations observed at these locations. Farther downstream, the fluctuations begin to decay, and the well-defined peak observed earlier becomes significantly reduced in magnitude. This is expected, because the sharp gradients observed in the mean axial profiles become less severe at these axial locations.

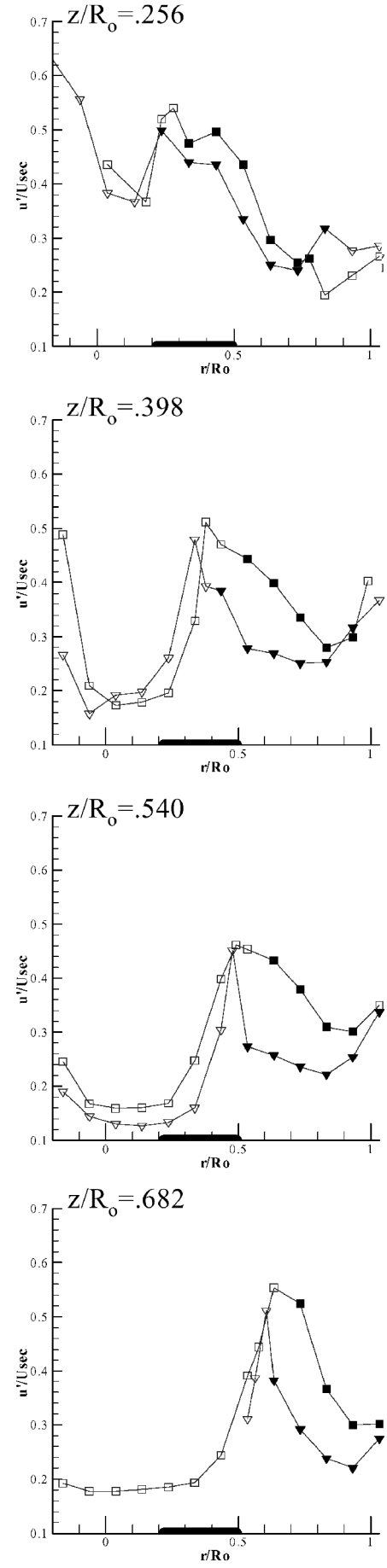

Fig. 21 Reacting flow rms axial velocity, U_{sec} = 11 m/s, secondary airflow velocity: solid symbols, no seeding; ■, no control; and ▼, control.

The reductions in the axial rms fluctuations with control is quite significant in the shear layer region with reductions greater than 50%. The spectra of the instantaneous velocity profile showed a strong peak near 200 Hz, indicating that the flow fluctuations are characterized by coherent oscillations in the flow. With control, the velocity spectra shows nearly a fivefold reduction in the peak value. This indicates that control is responsible for significantly reducing the coherent fluctuations (at the instability frequency of 200 Hz) in the flow. These significant reductions in velocity fluctuations are associated with the reductions in the pressure oscillations observed with control.

Conclusions

In this paper, the instability characteristics of a swirl-stabilized spray combustor have been determined, and a phase-delay feedback-loop controller has been implemented through a microprocessor. The effects of the phase-delay controller on both the combustion oscillations, as well as on the emissions, are examined. Two specific flow conditions, one corresponding to high NOx and the second corresponding to high-pressure oscillations, were selected for feedback-loop control studies. The following are the major conclusions of the present study.

1) The pressure oscillations in the combustor are influenced by both the equivalence ratio and the aerodynamic behavior of the fuel droplets represented by the primary-jet Reynolds numbers. In general, lower equivalence ratios and higher primary-jet Reynolds numbers led to stronger oscillations.

2) The dominant instability is at 200 Hz and represents a quarter-wave longitudinal mode.

3) Best control was achieved for a phase delay of 60–90 deg and resulted in a significant reduction in the pressure oscillations without adversely effecting emissions. Worst control was obtained between 240–270 deg and led to a significant increase in the pressure oscillations.

4) For the high NOx baseline case, best control led to a modest reduction of the pressure oscillations (around 30%), but this was accompanied by a nearly 40% reduction of NOx levels.

5) For the high-pressure oscillation case, the 200-Hz oscillation was reduced nearly threefold with 60-deg phase lag. However a secondary mode was enhanced, and the effective reduction in the pressure oscillations was around 50%. This reduction in pressure oscillation was not associated with any adverse effects on the emissions.

6) It is shown that, with control, the recirculation region is stronger (higher negative velocities). This contributes to the improved stabilization associated with control. Because a stronger recirculation can be induced by increasing swirl, this indicates the potential of passively controlling instabilities through control of the swirl strength in the combustor.

7) The peak axial velocities are reduced with control, and there is greater radial spread and improved mixing in the near field of the controlled combustor. These factors also contribute to improved flame stabilization.

8) The peak axial rms fluctuations for the reacting flow occur at the same radial location as the inflection point between the inner recirculation zone and outer shear layer region. These large fluctuations are attributed to strong interactions between the unburned droplets and hot recirculating combustion gases. The application of control resulted in a significant reduction of the peak velocity fluctuations at all axial locations. Thus, control reduces the destabilizing effects associated with high-amplitude fluctuations that appear in the uncontrolled case.

Acknowledgments

This work was supported by funds received from the propulsion program of the Office of Naval Research under Grant N00014-97-0957. Partial support, received from the National Aeronautics and Space Administration and the Louisiana Educational Quality Support Fund program, is also acknowledged.

References

[1]Rayleigh, J. W. S., *The Theory of Sound*, 2nd ed., Vol. 1, 1945.

[2]Lang, W., Poinsot, T., and Candel, S., "Active Control of Combustion Instability," *Combustion and Flame*, Vol. 70, 1987, pp. 281–289.

[3]Bloxsidge, G. J., Dowling, A. P., Hooper, N., and Langhorne, P. J., "Active Control of Reheat Buzz," *AIAA Journal*, Vol. 26, No. 7, 1988, pp. 783–790.

[4]Gulati, A., and Mani, R., "Active Control of Unsteady Combustion-Induced Oscillations," *Journal of Propulsion and Power*, Vol. 8, No. 5, 1992, pp. 1107–1115.

[5]Richards, G. A., and Janus, M. C., "Characterization of Oscillations During Premix Gas Turbine Combustion," *Transactions of the American Society of Mechanical Engineers*, Vol. 120, 1998, pp. 294–302.

[6]Schadow, K. C., Gutmark, E., Parr, D. M., Parr, T. P., Wilson, K. J., and Ferrell, G. B., "Enhancement of Fine Scale Turbulence for Improving Fuel Rich Plume Combustion," *Journal of Propulsion and Power*, Vol. 6, No. 4, 1990, pp. 357–363.

[7]Yu, K., Wilson, K. J., and Schadow, K. C., "Active Combustion Control in a Liquid-Fueled Dump Combustor," AIAA Paper 97-0462, Jan. 1997.

[8]Yu, K., Wilson, K. J., and Schadow, K. C., "Scale-Up Experiments on Liquid-Fueled Active Combustion Control," AIAA Paper 98-3211, July 1998.

[9]McManus, K. R., Poinsot, T., and Candel, S. M., "A Review of Active Control of Combustion Instabilities," *Progress in Energy and Combustion Science*, Vol. 19, 1993, pp. 1–29.

[10]Candel, S. M., "Combustion Instabilities Coupled by Pressure Waves and Their Active Control," Invited Lecture, *Twenty-Fourth Symposium (International) on Combustion*, Combustion Inst., Pittsburgh, PA, 1998, pp. 1277–1296.

[11]Gutmark, E., Parr, T. P., Hanson-Parr, D. M., and Schadow, K. C., "Evolution of Vortical Structure in Flames," *Twenty-Second Symposium (International) on Combustion*, Combustion Inst., Pittsburgh, PA, 1997, pp. 523–529.

[12]Gutmark, E., Parr, T. P., Hanson-Parr, D. M., and Schadow, K. C., "Closed-Loop Amplitude Modulation Control of Reacting Premixed Turbulent Jet," *AIAA Journal*, Vol. 29, No 12, 1991, pp. 2155–2169.

[13]Gutmark, E., Parr, T. P., Hanson-Parr, D. M., and Schadow, K. C., "Structure of a Controlled Ducted Flame," *Combustion Science and Technology*, Vol. 87, 1997, pp. 217–239.

[14]Schadow, K. C., Gutmark, E., and Wilson, K. J., "Active Combustion Control in a Coaxial Dump Combustor," *Combustion Science and Technology*, Vol. 81, 1992, pp. 285–300.

[15]McManus, K. R., Magill, J. C., Miller, M. F., and Allen, M. G., "Closed-Loop System for Stability Control in Gas Turbine Combustors," AIAA Paper 97-0463, Jan. 1997.

[16]Neumeier, Y., and Zinn, B. T., "Active Control of Combustion Instabilities Using Real Time Identification of Unstable Combustor Modes," *IEEE Transactions*, Vol. 40, 1995, pp. 691–698.

[17]Neumeier, Y., Markopoulos, N., and Zinn, B. T., "A Procedure for Real-Time Mode Decomposition, Observation, and Prediction for Active Control of Combustion Instabilities," *Proceedings of the 1997 IEEE Conference on Control Applications*, TP03, Inst. of Electric and Electrical Engineers, New York, 1997, pp. 818–823.

[18]Richards, G. A., Yip, M. J., Robey, E., Cowell, L., and Rawlins, D., "Combustion Oscillation Control by Cyclic Fuel Injection," *Journal of Engineering for Gas Turbines and Power*, Vol. 119, 1997, pp. 1–4.

[19]Richards, G. A., Janus, M. C., Robey, E., Cowell, L., and Rawlins, D., "Control of Flame Oscillation with Equivalence Ratio Modulation," *Journal of Propulsion and Power*, Vol. 15, 1999, pp. 232–240.

[20]Sivasegaram, S., and Whitelaw, J. H., "The Influence of Swirl on Oscillations in Ducted Premix Flames," *Combustion Science and Technology*, Vol. 85, 1991, pp. 195–205.

[21]Stephens, J. R., Acharya, S., Gutmark, E. J., Allgood, D. C., and Murugappan, S., "Open Loop Control of a Swirl-Stabilized Liquid Fuel Diffusion Flame," AIAA Paper 98-0351, Jan. 1998.

[22]Paschereit, C. O., Weisenstein, W., and Gutmark, E. J., "Role of Coherent Structures in Acoustic Combustion Control," AIAA Paper 98-2433, June 1998.

[23]Paschereit, C. O., Gutmark, E. J., and Weisenstein, W., "Control of Thermoacousic Instabilities in a Premixed Combustor by Fuel Modulation," AIAA Paper 99-0711, Jan. 1999.

[24]Cohen, J. M., Rey, N. M., Jacobson, C. A., and Anderson, T. J., "Active Control of Combustion Instability in a Liquid-Fueled Low-NOx Combustor," International Gas Turbine and Aerospace Congress and Exhibition, Paper 98-GT-267, 1998.

[25]Hibsham, J. R., Cohen, J. M., Banaszuk, A., Anderson, T. J., and Alholm, H. A., "Active Control of Combustion Instability in a Liquid-Fueled Sector Combustor," International Gas Turbine and Aerospace Congress and Exhibition, Paper 99-GT-215, 1998.

[26]Sivasegaram, S., and Whitelaw, J. H., "Control of Combustion and Emissions," *Proceedings of the 7th ONR Propulsion Meeting*, 1994, pp. 34–41.

[27] Sivasegaram, S., Tsai, R. F., and Whitelaw, J. H., "Control of Oscillations and NOx Concentrations in Ducted Premixed Flames by Spray Injection of Water," *American Society of Mechanical Engineers Symposium on Fire and Combustion*, 1995.

[28] Ghaffarpour, M., and Chehroudi, B., "Experiments on Spray Combustion in a Gas Turbine Model Combustor," *Combustion Science and Technology*, Vol. 92, 1993, pp. 173–200.

[29] Presser, C., Gupta, A. K., and Semerjian, H. G., "Aerodynamic Characteristics of Swirling Spray Flames: Pressure-Jet Atomizer," *Combustion and Flame*, Vol. 92, 1992, pp. 25–44.

[30] de La Rosa, A. B., Wang, G., and Bachalo, W. D., "The Effect of Swirl on the Velocity and Turbulence Fields of a Liquid Spray," *Transactions of the American Society of Mechanicl Engineers*, Vol. 114, 1992, pp. 72–81.

[31] Bulzan, D., "Velocity and Drop Size Measurements in a Confined, Swirl-Stabilized, Combusting Spray," *32nd AIAA/ASME/SAE/ASEE Joint Propulsion Conference*, July 1996.

[32] Durbin, M. D., Vangsness, M. D., Ballal, D. R., and Katta, V. R., "Study of Flame Stability in a Step Swirl Combustor," *Transactions of the American Society of Mechanicl Engineers*, Vol. 118, 1996, pp. 308–315.

[33] Aung, K., Liang, S., Seitzman, J., and Jagoda, J., "Measurements of Spray Properties and Mixing in a Simulated Combustor," *36th Aerospace Meeting and Exhibit*, Jan. 1998.

[34] Messina, T., and Acharya, S., "Characteristric of a Two-Phase Spray Issued from Asymmetric Nozzles," *4th International Conference on Multiphase Flows*, May–June 2001.

[35] Yanta, W. J., Smith, and Russell, R. A., "Measurements of Turbulence–Transport Properties with a Laser Doppler Velocimeter," AIAA Paper 73-169, Jan. 1973.

[36] Bracco, F. V., "Standing Acoustic Waves in a Confined Non-Uniform Gas," *Journal of Sound and Vibration*, Vol. 41, No. 3, 1975, pp. 301–309.

[37] Ando, Y., *Acustica*, Vol. 22, 1969, pp. 219–225.